

Experimental Evidence of Lateral Skin Strain During Tactile Exploration

Vincent Levesque and Vincent Hayward

Center for Intelligent Machines
Department of Electrical and Computer Engineering, McGill University
3480 University Street, Montréal, Qc, H3A 2A7, Canada
{vleves,hayward}@cim.mcgill.ca

Abstract. This paper describes an experimental platform for the study of stretch and compression of the human fingerpad skin during tactile exploration. A digital camera records the sequence of patterns created by a fingertip as it slides over a transparent surface with simple geometrical features. Skin deformation is measured with high temporal and spatial resolution by tracking anatomical landmarks on the fingertip. Techniques adapted from the field of online fingerprinting are used to acquire high-contrast fingerprint images and extract salient features (pores, valley endings, and valley bifurcations). The results of experiments performed with surfaces with a bump or hole and flat surfaces are presented. This work is motivated by the need to provide meaningful ‘tactile movies’ for a tactile display that uses distributed lateral skin stretch.

1 Introduction

Effective graphic displays rely on several illusions such as the fusion of a sequence of stills into a continuous flow. While the stimulus to which vision responds is well known, the exact nature of the relation between the mechanical signals on the skin and tactile perception is the subject of debate. This, as well as numerous technical challenges, makes the design of effective tactile displays an arduous task.

The work that follows is motivated in part by the need to improve our understanding of the mechanical behavior of the fingerpad as well as of the relation between mechanical signals and tactile perception. The immediate motivation, however, is the need to generate driving signals for the STReSS, a tactile display that relies on distributed lateral skin strain patterns to cause tactile sensations [8]. Previous attempts to drive a similar tactile display used an empirical approach to discover interesting tactile stimuli [4]. The work presented here uses an alternative approach that aims to create ‘tactile movies’, i.e. driving signals, from direct observation of the fingerpad deformations during tactile exploration given the unavailability of reliable biomechanical models at the scale of interest.

This paper proposes a skin deformation measurement technique that relies on the tracking of anatomical landmarks of a fingertip sliding over a transparent surface which can be flat or have simple geometrical features. Techniques

adapted from the field of online fingerprinting are used to acquire high-contrast fingerprint images and extract salient features resulting from anatomical landmarks as they contact a surface: pores, valley endings, and valley bifurcations. Further processing involving the computation of a triangulation of these features is then used to evaluate skin strain variations over time. Experiments were conducted with three types of surfaces: a surface with a bump, a surface with a hole, and a flat surface.

2 Previous Work

Much work was done in the recent past to observe, measure, and model the mechanical characteristics of the fingertip. Srinivasan proposed a ‘waterbed’ model of the fingertip consisting of a thin membrane enclosing incompressible fluids [12]. The predictions of the model were compared with pictures of skin indentation under a line load. Srinivasan and Dandekar developed four models of the primate fingertip using finite element methods [13]. The most complex model assumes a cylindrical shape with a rigid fingernail covering a third of its surface, and a rigid bone in its interior. Pawluk and Howe also studied the dynamic, distributed pressure response of the fingertip as it is loaded by a flat surface and developed a model based on their observations and measurements [9]. Dandekar and Srinivasan used videomicroscopy to observe and measure deformation of the skin under various static loads (such as a rectangular or cylindrical bar) [2]. Approximately 100-150 markers were applied to the fingertip using a micro tip pen and located manually in the images to verify the predictions of skin models.

Fingertip deformation was also studied in the context of fingerprint recognition. Dorai, Ratha and Bolle relied on local motion data embedded into an MPEG- $\{1,2\}$ video stream to detect distortion in a sequence of fingerprint images and select optimal fingerprints [3]. Cappelli, Maio and Maltoni proposed a model of non-linear fingerprint deformations that segments the fingertip in three regions: a stationary inner region, a free outer region, and an intermediate region that stretches and compresses [1].

3 Skin Strain Measurement Technique

The measurement platform uses techniques inspired by the field of online fingerprinting to image moving fingerprints in contact with simple surfaces (Section 3.1) and extract anatomical landmarks (Section 3.2). The extracted features are then tracked and processed, yielding a streams of relative local skin strain variations in time (Section 3.3).

3.1 Fingerprint Image Acquisition

Principle. A wide variety of fingerprint sensors have been developed for biometric applications including optical sensors, solid-state sensors (capacitive or

thermal) and ultrasound sensors [5]. Few of these are appropriate for the purpose of fingerpad deformation analysis which requires a high spatial and temporal resolution as well as imaging through a non-flat contact surface. Prism-based fingerprint capture is the most straightforward method.

Figure 1(a) illustrates the principle used by a typical prism-based fingerprint sensor. The frustrated total internal reflection results in a high-contrast pattern of black ridges over a white background. Non-flat contact surfaces, however, break the frustrated total internal reflection as illustrated in Figure 1(b). Placing a diffuser on the entry face of the prism creates an illumination field with uniformly distributed optical path directions and restores the frustrated total internal reflection by insuring that at least one ray is reflected toward the camera for each position on the surface (Figure 1(c)). The size of the diffuser limits the angles at which light can strike the surface and thus imposes constraints on the surface gradients. It can be shown that these constraints practically limit variation in the surface to one dimension. The local gradient of the surface must further be limited to a reasonable range. Please see [6] for details.

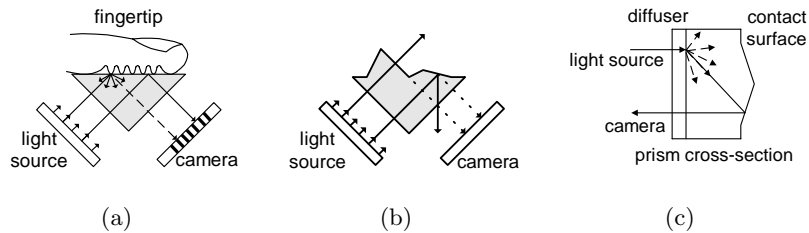


Fig. 1. Typical prism-based fingerprint sensor. (a) The contact between fingerprint ridges and the surface causes light to be scattered. The absence of contact at fingerprint valleys causes light to be reflected. (b) A high surface gradient causes light to escape the prism. A low surface gradient causes light to be reflected away from the camera. (c) A diffuser creates a near-Lambertian light source that enables the use of non-flat contact surfaces.

Experimental Platform. The experimental platform is seen in Figure 2. An opal diffuser is attached to a 50 mm × 50 mm × 70 mm BK7 right-angle prism. Two parallel ruled surfaces were machined onto the surface of thin BK7 glass plates: a surface with a bump and a surface with a hole, both having a Gaussian profile with a height of 0.5 mm and a width of 3 mm. Plates are joined with the prism using an index matching liquid (Cargille Immersion Oil Type A).

A powerful light source was assembled using a 250W/120V halogen lamp to insure a sufficient depth of field to maintain focus on the slanted fingerpad. A monochrome progressive scan CCD camera (Pulnix TM-6703) with an 8-bit pixel depth and a resolution of 640 × 484 at 60 Hz is rotated to yield approximately

the same resolution in x and y despite the perspective view of the fingertip. A zoom (Navitar Zoom 7000) allows the imaging system to focus on a region of approximately $10\text{ mm} \times 10\text{ mm}$. Images are acquired by a frame grabber (Matrox Meteor-II/MC) and processed with software built using the Matrox Imaging Library (MIL) and the Computational Geometry Algorithms Library (CGAL).

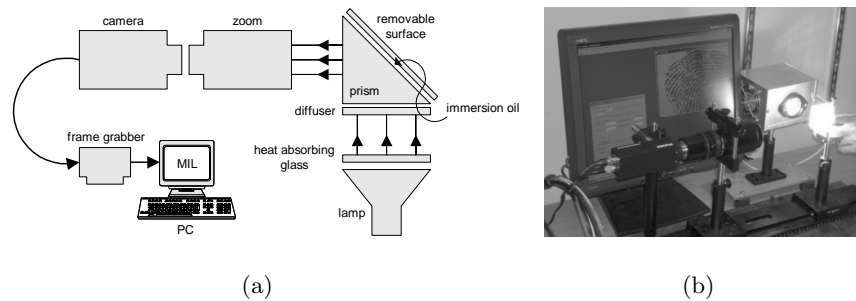


Fig. 2. Experimental platform: (a) illustration, and (b) picture.

Corrections. Geometric distortions are corrected by imaging a precise calibration grid consisting of dots spaced by 0.5 mm printed on a sheet of transparency film. The pattern resulting from the application of the grid on the contact surface with a thin oil film is analyzed to correct the perspective projection, ‘unroll’ the contact surface, and measure pixel size. The intensity of fingerprint valleys is also normalized to compensate for illumination non-uniformity.

3.2 Feature Extraction

Online fingerprint recognition generally relies on two types of salient features of the fingerprint called minutiae: ridge endings and ridge bifurcations [5]. Roddy and Stosz proposed the use of pores to increase matching accuracy [11]. Pores are small openings on the surface of the fingerprint ridges with a density of approximately 5 per mm^2 [11]. The following feature extraction process is based on their work. The process, illustrated in Figure 3, extracts valley endings, valley bifurcations, and pores.

Fingerprint images are first smoothed with a Gaussian filter to reduce noise. The local average in a square window of a given width (approx. 2 mm) is then computed for each pixel. A high local average and a low local variance are then used as an indicator of background pixels (similar to [7]). A binarization operation then uses the local average map as a pixel-wise threshold on the foreground image to segment valley and pore pixels (white) from ridge pixels (black).

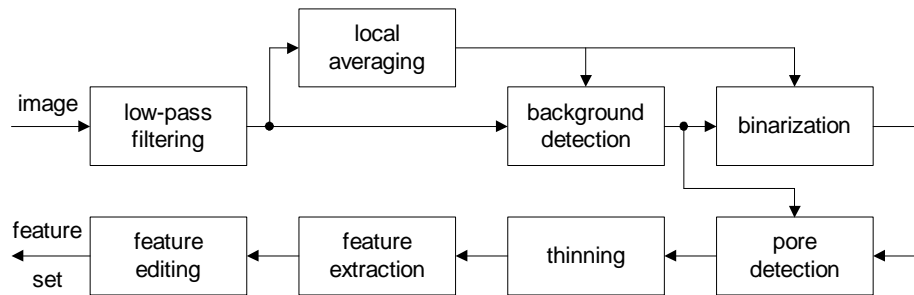


Fig. 3. Feature extraction block diagram.

Pores are round with a diameter varying between 88 and 220 μm [10] and can thus be detected from the binary fingerprint by connected-component (or blob) analysis. A blob — defined as a set of white pixels in which every pixel is 4-connected to at least one other pixel — is considered to be a pore if its area is smaller than 0.2 mm^2 . The position of a pore is determined by computing its center of mass using grayscale intensity values from the foreground image.

A thinning operation reduces the remaining valley pattern to a width of 1-pixel while maintaining its topology. The number of 8-neighbors of skeleton pixels is then used to determine their classification as illustrated in Figure 4(a). Illustrations shown in this paper represent pores as circles, valley endings as squares, and valley bifurcations as triangles. The orientation of nearby valleys is used to obtain distinguishing minutia characteristics as illustrated in Figures 4(b) and 4(c). Pores do not have reliable distinguishing features.

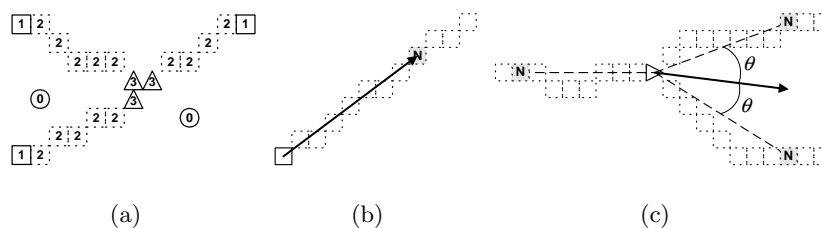


Fig. 4. Minutiae extraction: (a) pixel classification based on number of 8-neighbors (pore: 0; valley ending: 1; valley: 2; valley bifurcation: 3 or more), (b) orientation of valley endings, and (c) orientation of valley bifurcations.

The feature extraction process often results in fingerprint skeleton artifacts. Syntactic editing rules adapted from [11] are applied to eliminate the four common artifacts shown in Figure 5. Short valleys, spurs and bridges are replaced by pores. Broken valleys are bridged. Two extra filtering operations are applied

to reject unreliable features. The first operation discards features in regions of high feature density. The second operation rejects features near the outer border of the fingerprint. Readers are referred to [6] for detailed explanations. Figure 6 illustrates the feature extraction process in a fingerprint segment.



Fig. 5. Artifacts: (a) short valley, (b) broken valley, (c) spur, and (d) bridge.

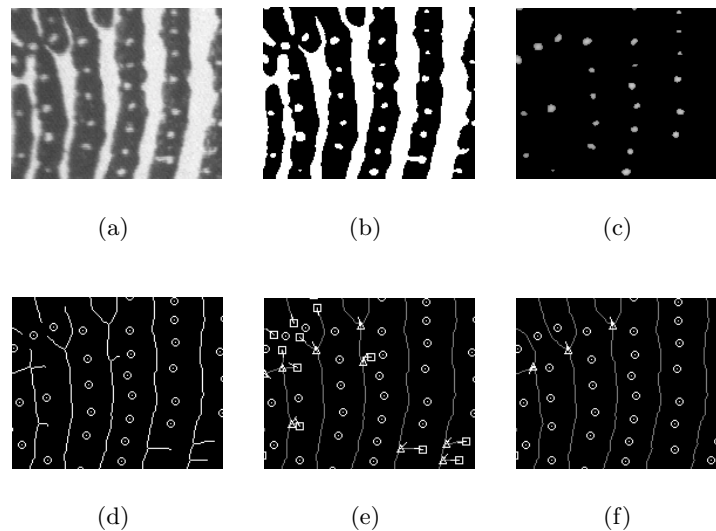


Fig. 6. Feature extraction in fingerprint segment: (a) grayscale fingerprint, (b) binarized fingerprint, (c) grayscale pores (d) thinned skeleton with pores, and (e) extracted features with minutiae orientation before and (f) after corrections.

3.3 Skin Strain Measurement

Skin strain measurement consists of three steps. The first step matches features in pairs of consecutive frames. The second step assembles matches into smooth and reliable feature trajectories. The third step infers changes in skin strain from the relative changes in edge length in a triangulation of tracked features.

Feature Matching. Feature matching relies on the assumption that the image acquisition rate is sufficiently high to ensure that feature displacements are much shorter than inter-feature distances. For each pair of frames, an attempt is made to match as many features as possible from the first frame to the second. Matching is performed by searching for the best match near a feature's expected position as predicted from its previous displacement, if available. Any feature of the same type (valley ending, valley bifurcation or pore) within a given radius (approx. 0.3 mm) is considered a candidate match and given a confidence rating that decreases with the distance from the feature's expected position and with the minutia orientation error, if applicable. Matches are selected so as to maximize the sum of confidence ratings without matching the same feature twice. Figure 7 shows examples of successful and unsuccessful matching attempts.

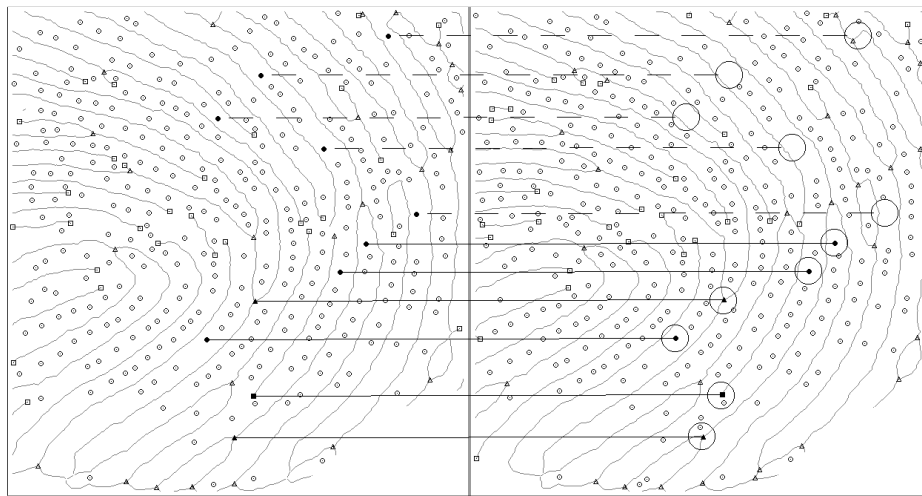


Fig. 7. Selected matched (full lines) and unmatched (dashed lines) features.

Feature Tracking. Fingerprint feature extraction algorithms are not sufficiently reliable to insure the stability of features. As a result, the matching algorithm is generally capable of tracking features continuously only for a number of frames. No attempt is made to keep track of features through discontinuities. The result is a set of disjoint feature trajectories starting and ending at different frames. To improve the quality of measurements, features trajectories that do not span a minimal number of frames (approx. 30) are assumed to be unreliable and rejected. The discrete nature of the image grid as well as minor feature extraction errors also result in jagged feature trajectories. This problem is corrected by smoothing trajectories, resulting in sub-pixel feature coordinates.

Measurement. Changes in local skin strain are estimated by observing changes in a triangulation of tracked features. The subset of features of a frame that are tracked in the subsequent frame is used to construct a Delaunay triangulation (e.g. Figure 8(a)). The triangulation is maintained in the second frame. The change in local skin strain is evaluated by measuring the change of edge lengths as illustrated in Figure 8(b). Each pair of successive images is analyzed, yielding a map of relative changes in skin strain over time. Skin strain measurements are illustrated by variations in the grayscale intensity of edges from black (maximum relative decrease in length) to white (maximum relative increase) (Figure 8(c)). Measurements can also be made over a span of more than one frame.

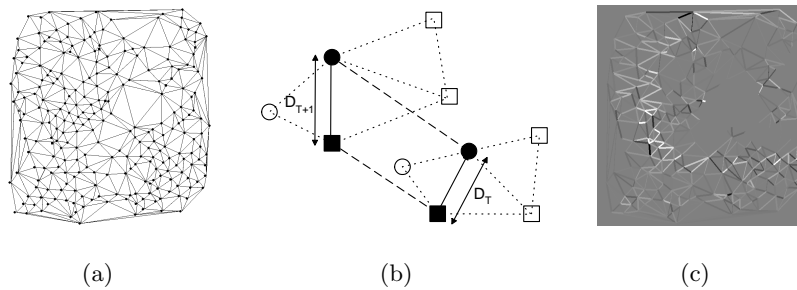


Fig. 8. Skin strain measurement: (a) typical triangulation of tracked features, and (b) edge length changes computation, (c) example of edge length changes (white/black= $\pm 5\%$).

4 Experimental Results

All experiments were performed with the same fingertip. Each sequence contains 180 frames (3 seconds at 60 frames/second). Images measure approximately $10.3 \text{ mm} \times 10.9 \text{ mm}$ after calibration. Section 4.1 presents interesting results obtained with flat surfaces. Section 4.2 presents results obtained while sliding over a hole or a bump.

4.1 Flat Surface

Measurements obtained from movement over flat surfaces are generally difficult to interpret. This section provides interesting measurements obtained from image sequences for which a meaningful interpretation could be found. In the first example, a fingertip is pressed against the surface and rotated. In the second example, a fingertip is moved back and forth horizontally.

Rotation. In this example a fingertip is pressed firmly against a flat surface and rotated. At frame 70, the fingertip begins a counter-clockwise rotation. Most of the fingertip is sticking to the glass (Figure 9(a)). The top part of the finger is moving up, stretching the intermediate zone between the moving and non-moving segments. The right-hand part is moving toward the upper-left corner, resulting in compression at the junction of the moving and non-moving parts. Changes in triangulation edge lengths from frame 70 to 71 (Figure 9(b)), and from frame 70 to 76 (Figure 9(d)) agree with these observations. Notice that the fingerprint seems to be expanding vertically but compressing horizontally.

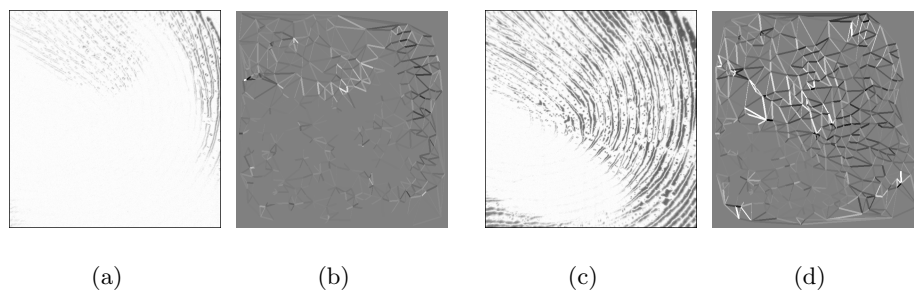


Fig. 9. Rotation of the fingertip: (a) frame difference and (b) measurements (white/black= $\pm 10\%$) from frame 70 to 71; (c) frame difference and (d) measurements (white/black= $\pm 20\%$) from frame 70 to 76.

Lateral Movement. In this example a finger pressed against a flat surface moves back and forth horizontally. A patch of skin is sticking to the glass while the surrounding skin moves with the finger. Figure 10(a) shows a sequence of images in which the fingertip is returning from the left. Figure 10(c) shows the variations in edge lengths from frame 30 to 31, near the end of this sequence. The center of the fingertip is stationary while the sides are moving right (Figure 10(b)) resulting in compression to the left and expansion to the right.

4.2 Bump/Hole Surfaces

Experiments were conducted with three contact surfaces: a flat surface, a surface with a bump, and a surface with a hole (see Section 3.1). The fingertip was moved from left to right at an average speed varying from 2.0 to 2.8 mm/s. Figure 11 illustrates a single measurement between successive frames for each surface. The approximate width and position of the 0.5 mm high/deep Gaussian shapes is indicated by two dotted lines separated by 3 mm on fingerprint images. While no pattern emerges from the flat surface, a tendency of compression can be observed on the left and a tendency of expansion on the right of the bump. The

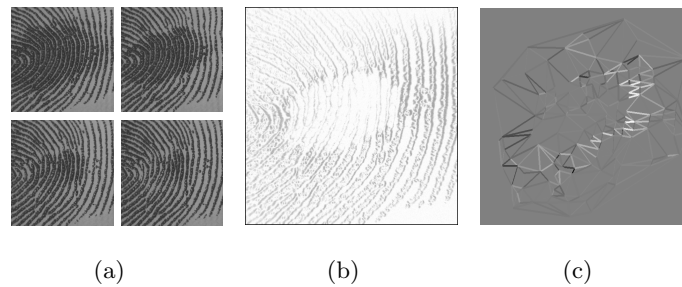


Fig. 10. Lateral movement of fingertip: (a) frames 26, 28, 30 and 32, (b) frame difference and (c) measurements (white/black= \pm 30%) from frame 30 to 31.

reverse can be observed in the case of a hole. Measuring the change in edge length over a span of 10 frames provides cleaner results as shown in Figure 12.

5 Discussion and Future Work

The patterns of compression and expansion resulting from the presence of a bump or hole are in agreement with our intuition. These patterns, however, are barely discernible. Measurements made with a flat surface show that significant deformations are present even in the absence of a shape. It is unclear at this point whether these measurements are representative of the actual deformations of the fingertip (such as stick-slip of the fingertip ridges) or due to measurement errors and noise.

The signal-to-noise ratio is low. The triangulation shown in Figure 11(d), for example, has an average edge length of 48 pixels. An error of one pixel thus causes an error of approximately 2% in the relative length change. Such an error is significant when considering the range of relative changes observed (maximum of 5% to 15%). The improvement in pattern clarity when measuring through extended periods is also consistent with the presence of noise. An increase in camera resolution could possibly reduce the noise significantly but the noise may also be inherent to the contact-based imaging technique used.

It is important to mention that excessive pressure must generally be applied by the fingertip to avoid losing contact with the surface as shown in Figure 13. This limitation, as well as limitations in the shapes and materials used, could be removed by using a different imaging system such as ultrasounds.

The robustness of the image processing algorithm also requires improvements. The current algorithms function satisfactorily only for subjects with large, clearly visible pores. Improvements may be obtained by exploring computationally-intensive algorithms generally not considered for latency-sensitive biometric applications. Improvements to the tracking algorithm and calibration method are also planned. Finally, a recently completed prototype of the STReSS tactile dis-

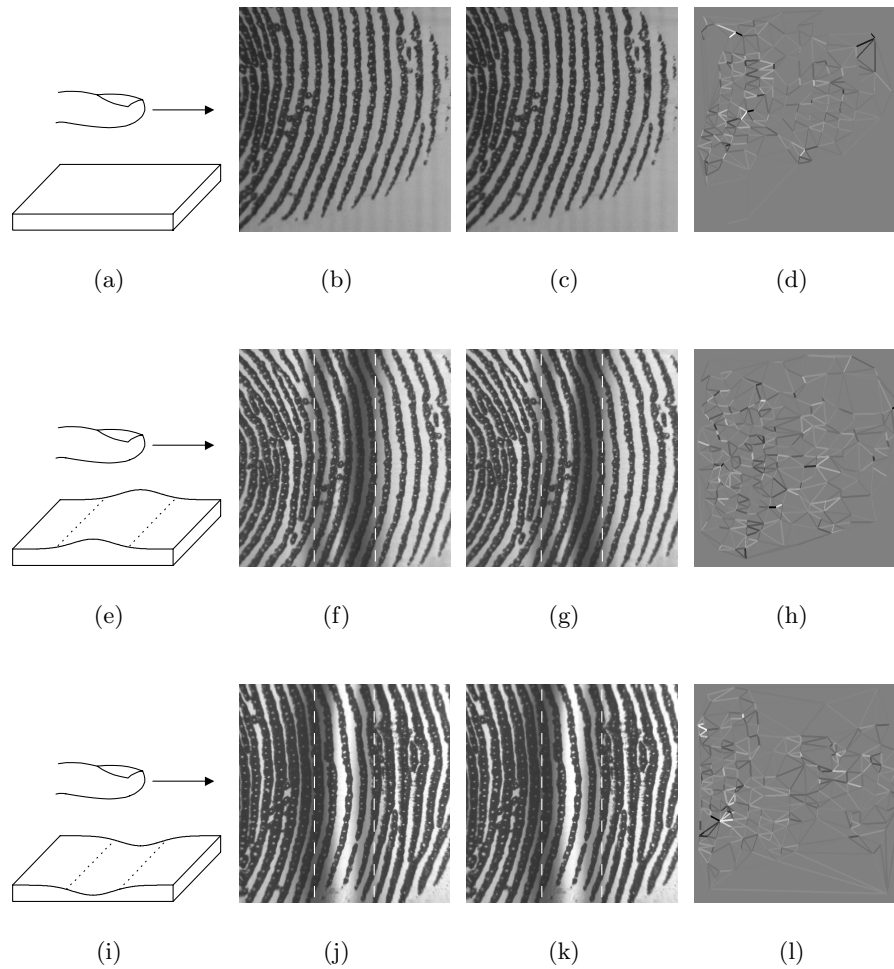


Fig. 11. Measurements between successive frames: (a)-(d) frame 115 to 116 on a flat surface, (e)-(h) frame 112 to 113 on a surface with a bump, and (e)-(h) frame 73 to 74 on a surface with a hole. From left to right: illustration (not to scale), first and second frames, and measurements (white/black= $\pm 5\%$).

play [8] will soon be used to experiment with mappings from measurements to ‘tactile movies’.

6 Acknowledgment

The authors would like to thank Don Pavlasek and Jozsef Boka (Mechanical Workshop, ECE dept., McGill) for their technical support. Many thanks also

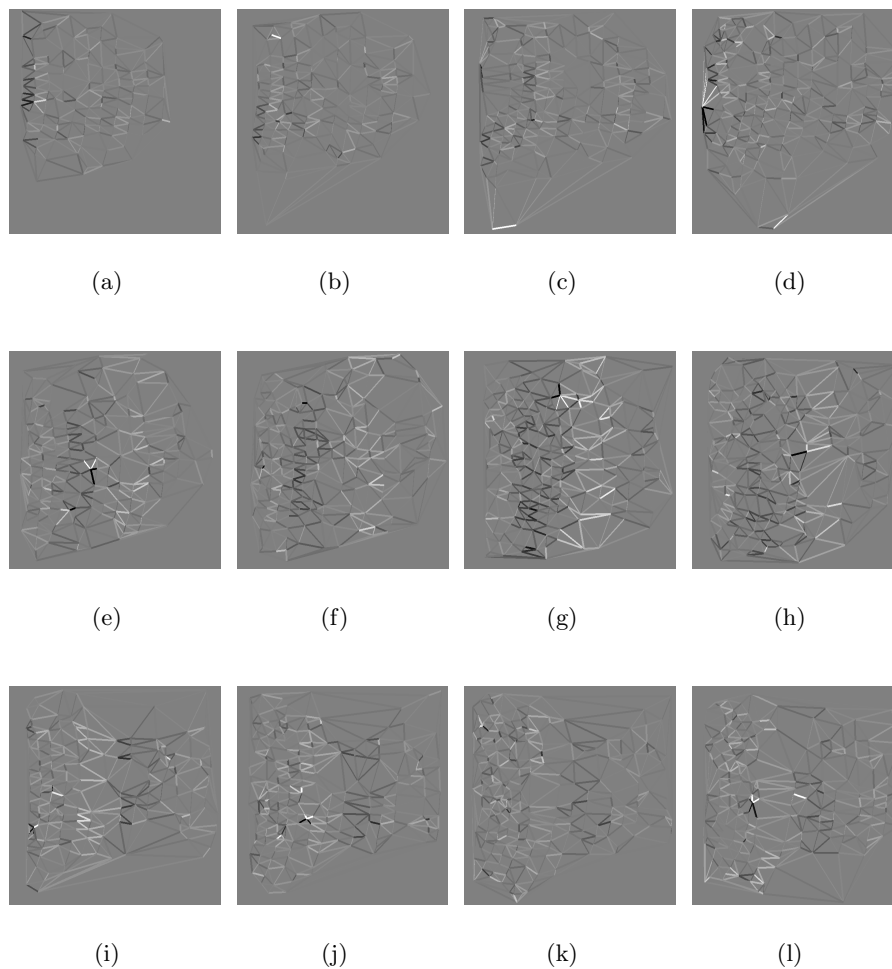


Fig. 12. Measurements over a span of 10 frames (white/black= $\pm 15\%$): (a)-(d) flat surface, (e)-(h) surface with a bump, and (i)-(l) surface with a hole. From left to right: measurements from frame 75 to 86, 100 to 111, 125 to 136, and 150 to 161.

to Jerome Pasquero for stimulating discussions and helpful comments. Financial support from the Institute for Robotics and Intelligent Systems (IRIS-III, Project HI-VEC) and from the Natural Sciences and Engineering Council of Canada (NSERC) is gratefully acknowledged.

References

1. R. Cappelli, D. Maio, and D. Maltoni. Modelling plastic distortion in fingerprint images. In *Proc. Second International Conference on Advances in Pattern Recog-*

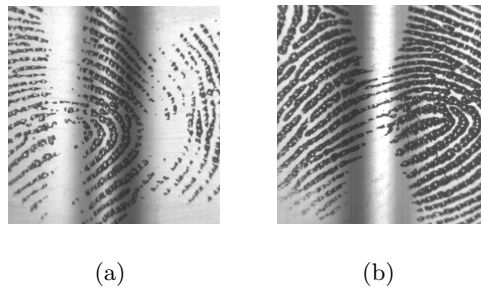


Fig. 13. Loss of contact while sliding over a shape: (a) bump, and (b) hole.

- inition (*ICAPR2001*), pages 369–376, Rio de Janeiro, March 2001.
2. K. Dandekar and M. A. Srinivasan. Role of mechanics in tactile sensing of shape. Touch Lab Report 2, RLE TR-604, MIT, Cambridge, 1997.
 3. C. Dorai, N. Ratha, and R. Bolle. Reliable distortion detection in compressed fingerprint videos. In *Proc. CVPR-2000*, Hilton Head SC, 2000.
 4. V. Hayward and M. Cruz-Hernandez. Tactile display device using distributed lateral skin stretch. In *Proc. of the Haptic Interfaces for Virtual Environment and Teleoperator Systems Symposium*, volume DSC-69-2, pages 1309–1314. ASME IMECE2000, Orlando, Florida, 2000.
 5. A. Jain and S. Pankanti. Automated fingerprint identification and imaging systems. In H. C. Lee and R. E. Gaensslen, editors, *Advances in Fingerprint Technology*. Elsevier, New York, second edition, 2001.
 6. V. Levesque. Measurement of skin deformation using fingerprint feature tracking. Master’s thesis, Dept. of Electrical and Computer Eng., McGill U., Nov. 2002.
 7. B. M. Mehre and B. Chatterjee. Segmentation of fingerprint images - a composite method. *Pattern Recognition*, 22(4):381–385, 1989.
 8. J. Pasquero and V. Hayward. STReSS: A practical tactile display with one millimeter spatial resolution and 700 Hz refresh rate. Accepted for EuroHaptics 2003.
 9. D. T. V. Pawluk and R. D. Howe. Dynamic contact of the human fingerpad against a flat surface. *Journal of Biomechanical Engineering*, 121(6):605–611, Dec. 1999.
 10. A. R. Roddy and J. D. Stosz. Fingerprint features — statistical analysis and system performance estimates. *Proc. of the IEEE*, 85(9):1390–1421, 1997.
 11. A. R. Roddy and J. D. Stosz. Fingerprint feature processing techniques and poroscopy. In L. C. Jain, U. Halici, I. Hayashi, and S. B. Lee, editors, *Intelligent Biometric Techniques in Fingerprint and Face Recognition*. CRC Press, Boca Raton, 1999.
 12. M. A. Srinivasan. Surface deflection of primate fingertip under line load. *J. Biomechanics*, 22(4):343–349, 1989.
 13. M. A. Srinivasan and K. Dandekar. An investigation of the mechanics of tactile sense using two dimensional models of the primate fingertip. *Journal of Biomechanical Engineering*, 118:48–55, 1996.